Supplementary Information

Rational design of the Z-scheme hollow structure Co$_9$S$_8$/g-C$_3$N$_4$ as an efficient visible light photocatalyst for tetracycline degradation

Xueying Wang, Rui Han, Hao Liu, Ximei Wang, Wei Qin, Chuannan Luo*

Key Laboratory of Interfacial Reaction & Sensing Analysis in Universities of Shandong, School of Chemistry and Chemical Engineering, University of Jinan, Jinan 250022, PR China

*Corresponding author: Tel.: +86 0531 89736065. Professor Chuannan Luo is the Corresponding author of this article.

E-mail address: chm_wangxy@ujn.edu.cn (Wang); chm_yfl518@163.com (Luo)

SI Synthesis of g-C$_3$N$_4$ nanosheets

g-C$_3$N$_4$ nanosheets were obtained by thermally polycondensing the inexpensive nitrogen-rich precursor melamine and then thermally etching in air. Specifically, 5 g of melamine was placed in a covered crucible and heated to 550 °C in a muffle furnace at a heating rate of 5 °C min^{-1}, maintaining the final temperature for 4 h. Then, the samples were transferred to a porcelain boat and heated to 500 °C in a muffle furnace at a heating rate of 10 °C min^{-1}, maintaining the final temperature for 2 h. The g-C$_3$N$_4$ nanosheets were obtained as yellow powders.

S2 Synthesis of c-CSCN

Starting with ZIF-67 as the template, c-Co$_9$S$_8$ was obtained by a sulfurisation reaction and calcination in inert gas. Then, g-C$_3$N$_4$ was coated onto the surface of the c-Co$_9$S$_8$ to obtain c-CSCN. Specifically, Co(NO$_3$)$_2$·6H$_2$O (175 mg) and 2-methylimidazole (320 mg) were each dissolved in 40 mL of methanol. Then, the two solutions were mixed quickly and aged at room temperature for 6 h. The purple precipitate generated (ZIF-67) was washed several times with ethanol and dispersed in 20 mL of ethanol for use. Next, 50 mg of thioacetamide (TAA) was dissolved in 10 mL of ethanol, and 10 mL of the ZIF-67 mixture prepared above was added to it. After being fully stirred, the resulting mixture was transferred to a Teflon-lined autoclave and heated in an air dry oven at 180 °C for 3 h. After cooling to room temperature, the precipitate was washed several times with ethanol and dried to obtain a cobalt sulphide product. c-Co$_9$S$_8$ was produced by annealing the cobalt sulphide product material under an argon stream at 550 °C for 6 h with a heating rate of 10 °C min^{-1}. Finally, an appropriate amount of the g-C$_3$N$_4$ nanosheets was dispersed in 25 mL of methanol. A homogeneous g-C$_3$N$_4$ suspension was obtained by ultrasonic dispersion. Subsequently, the c-Co$_9$S$_8$ prepared above was dispersed in the g-C$_3$N$_4$ suspension. The mixture was stirred at room temperature for 24 h and then dried in a vacuum oven at 60 °C to obtain c-Co$_9$S$_8$/g-C$_3$N$_4$ composite photocatalyst. In the same way, c-CSCN samples with different g-C$_3$N$_4$ loadings were obtained by changing the amount of g-C$_3$N$_4$ used (0, 33, 50, 66, 100 wt%). These samples were labelled c-

CSCN-x%, where x represents the mass percentage of g-C$_3$N$_4$ used. Furthermore, sheet-type Co$_9$S$_8$ (s-Co$_9$S$_8$) and its composites with g-C$_3$N$_4$ (s-CSCN-x%) were prepared for comparison with c-CSCN-x%.

S3 Synthesis of s-CSCN

Specifically, CoSO$_4$·7H$_2$O (0.879 g) was dissolved in 20 mL of ultrapure water, and Na$_2$SO$_3$ (0.326 g) was added under magnetic stirring. Then 15 mL of N$_2$H$_4$·H$_2$O (80%) was added and stirred for 30 min. The mixture was transferred to a Teflon-lined autoclave and kept in a air dry oven at 180 °C for 12 h. After cooling to room temperature, the precipitate was washed several times with ethanol and dried to obtain sheet-Co$_9$S$_8$ (s-Co$_9$S$_8$). Finally, an appropriate amount of the g-C$_3$N$_4$ nanosheets was dispersed in 25 mL of methanol. A homogeneous g-C$_3$N$_4$ suspension was obtained by ultrasonic dispersion. Subsequently, the s-Co$_9$S$_8$ was dispersed in the g-C$_3$N$_4$ suspension. The mixture was stirred at room temperature for 24 h and then dried in a vacuum oven at 60 °C to obtain s-Co$_9$S$_8$/g-C$_3$N$_4$ composite photocatalyst. In the same way, s-CSCN samples with different g-C$_3$N$_4$ loadings were obtained by changing the amount of g-C$_3$N$_4$ used (0, 33, 50, 66, 100 wt%). These samples were labelled s-CSCN-x%, where x represents the mass percentage of g-C$_3$N$_4$ used.

S4 Photoelectrochemical measurements

The photoelectrochemical properties of the samples were tested using a standard three-electrode method in photoelectrochemical system. The electrolyte was 0.1 M Na$_2$SO$_4$ solution. The ITO/catalysts electrodes served as the working electrode. Pt wire and Ag/AgCl electrode were used as the counter electrode and reference electrode, respectively. The photocurrent responses were measured at 0.0 V during on-off cycling irradiated by using a Xe lamp with 420 nm cutoff filters. Electrochemical impedance spectroscopy (EIS) was conducted at the open circuit potential with a frequency range of 0.1 Hz to 100 kHz. Mott-Schottky plots were obtained with a potential range from -1 V to 1 V (potential step: 10 mV) at frequencies of 2.0 and 2.5 kHz using EIS-300 software. Electron spin resonance (ESR) signals of superoxide (·O$_2$$^-$) and hydroxyl (·OH) radicals were studied on a

Bruker a300 spectrometer under dark and visible light irradiation conditions.

S5 Photocatalytic activity measurement

In order to evaluate the photocatalytic properties of the prepared samples, the photodegradation rate of tetracycline (TC) was measured under visible light irradiation. A 300 W Xe lamp (PLS-SXE300C) with a cutoff filter (400 nm) was used to obtain visible light. Photocatalytic degradation experiments were carried out in photocatalytic reactor. In a typical procedure, 10 mg photocatalysts were dispersed into 50 mL TC solution (25 mg L^{-1}). Prior to illumination, the suspension was magnetically stirred in dark for 30 min to establish an adsorption-desorption equilibrium. During photocatalytic reaction, samples were taken at specific time points and centrifuged to obtain the supernatant, and the concentration change before and after the degradation of TC was analyzed with an UV-2550 spectrophotometer and the total organic carbon (TOC) measurements were measured on a TOC analyzer (Shimadzu).

S6 Catalyst stability test

In order to test the stability of the catalyst after the completion of degradation experiment, the recycle text was researched via five times under the same conditions. In a typical procedure, 10 mg of photocatalyst was dispersed in 50 mL of TC solution (25 mg L^{-1}) as the first cycle experiment. All the catalysts were then collected and dispersed again into 50 mL TC solution (25 mg L^{-1}) for the next cycle of experiments. To further verify the stability of the sample, the collected catalyst was characterized by XRD.

S7 Detection of active species

The active species that contribute to the photocatalytic degradation process were identified via free radical capture texts. Benzoquinone (BQ), triethanolamine (TEOA) and isopropanol (IPA) were used as scavengers for superoxide radicals ($\cdot O_2^-$), hole (h^+) and hydroxyl radicals ($\cdot OH$), respectively. The capture agent was added to the catalyst-TC system before the photocatalytic degradation experiment, and the photocatalytic degradation experiment was carried out under the same conditions. The

concentration change before and after the degradation of TC was measured by a UV-2550 spectrophotometer and the TOC measurements were measured on a TOC analyzer (Shimadzu).

S8 Charge flow tracking by photodeposition

Using H_2PtCl_6 as a precursor, 1 wt% of Pt was photodeposited on the surface of c-CSCN-50%. Typically, 10 mg of c-CSCN-50% and a calculated amount of Pt precursor were mixed in 100 mL of deionized water with stirring. The suspension was then irradiated with a 300 W Xe lamp by cycle cooling water equipment. After 2 h of photodeposition, the suspension was filtered, washed several times with deionized water, and finally dried in a vacuum oven at 60℃ overnight.

Table S1 Surface areas and pore sizes for g-C_3N_4, c-CSCN-50%, and s-CSCN-50%

Sample	Surface area[a] (m^2/g)	Pore size[b] (nm)
g-C_3N_4	12.728	7.76
c-CSCN-50%	23.205	6.11
s-CSCN-50%	13.898	5.82

[a] Measured by the Brunauer-Emmett-Teller (BET) method.

[b] Pore diameters calculated form the desorption isotherms using the Barrett-Joyner-Halenda (BJH) model.
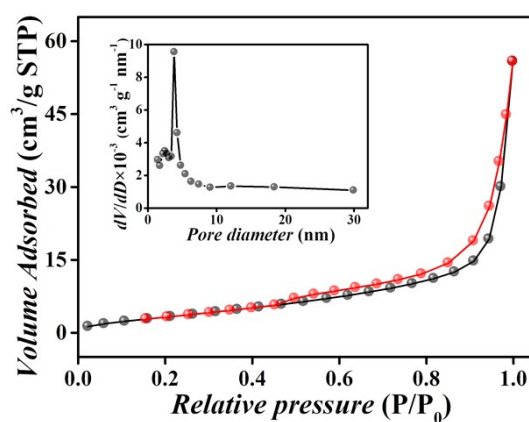
Fig. S1 N_2 adsorption-desorption isotherms and the corresponding pore size distributions (inset) for g-C_3N_4 and s-CSCN-50%.
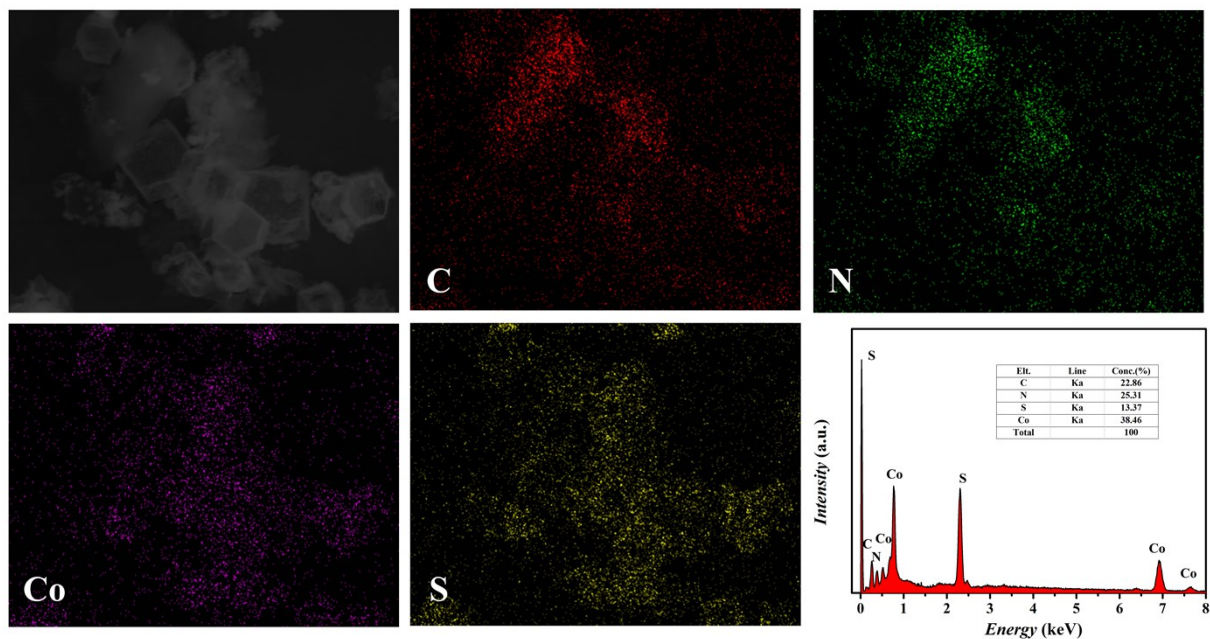
Fig. S2 Elemental mapping images (C, N, Co, and S) and EDS spectrum for c-CSCN-50%.
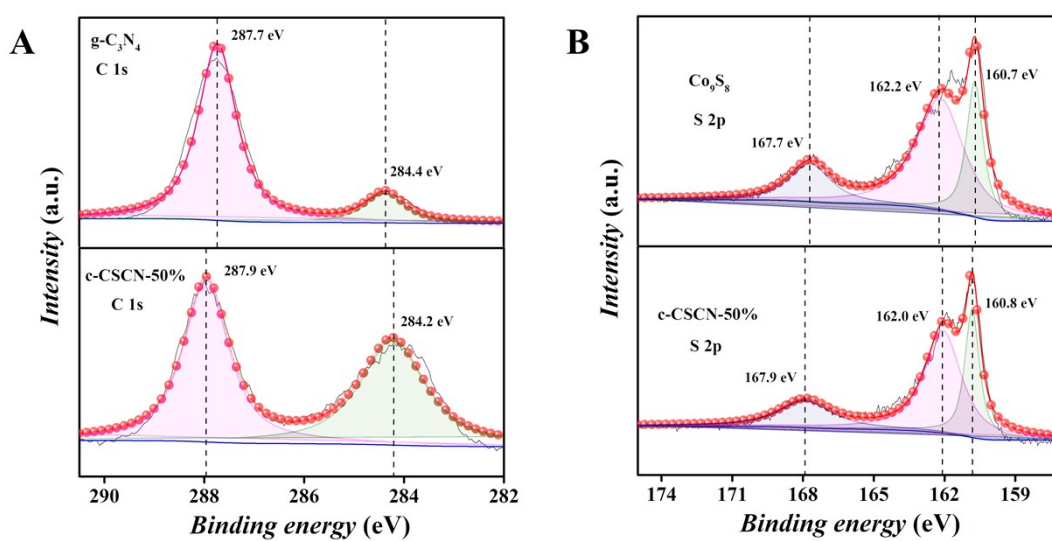
Fig. S3 C 1s (A) and S 2p (B) XPS spectra of the as-prepared materials.

Table S2 Pseudo-first-order reaction rate constants for the as-prepared samples

Samples	g-C$_3$N$_4$	c-CSCN-33%	c-CSCN-50%	c-CSCN-66%	c-Co$_9$S$_8$
k/min^{-1}	0.00586	0.02009	0.03494	0.02399	0.00207
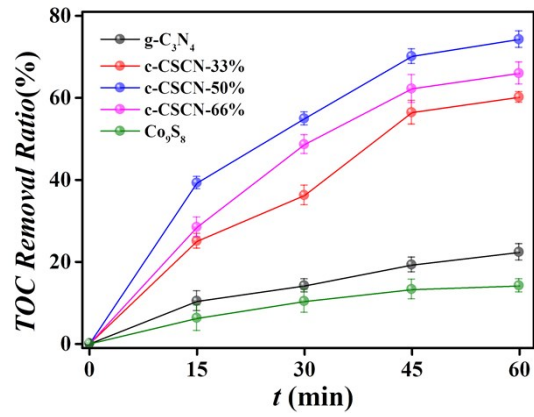
Fig. S4 TOC removal curves for several different reaction systems considered in this study.
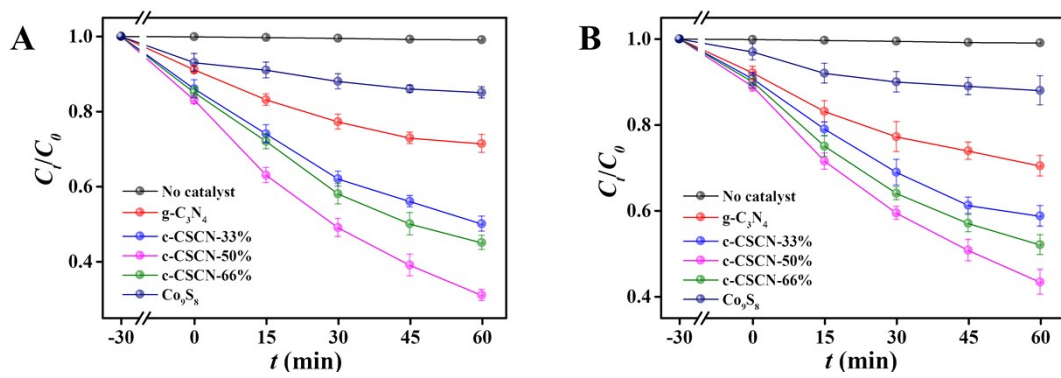
Fig. S5 Photodegradation of oxytetracycline (A) and chlorotetracycline (B) in different reaction

systems.
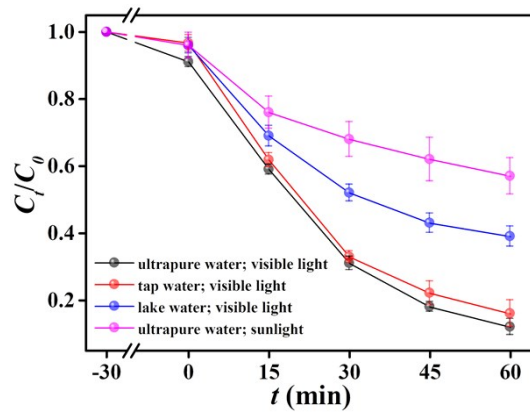
Fig. S6 Results for the real-world application of c-CSCN-50%.
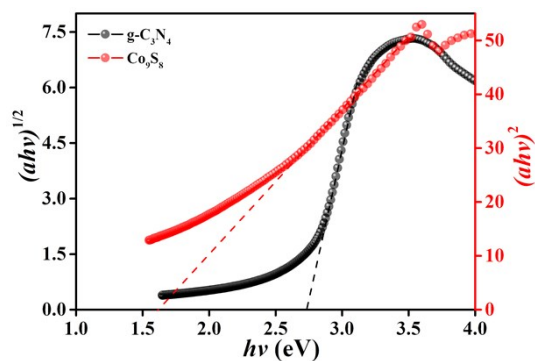
Fig. S7 $(\alpha h v)^2$ vs. photon energy curves for c-Co$_9$S$_8$, and $(\alpha h v)^{1/2}$ vs. photon energy curves for g-C$_3$N$_4$.
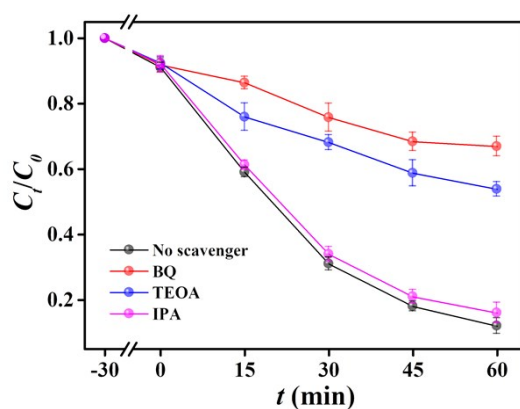
Fig. S8 Results for the active-substance capture experiments for c-CSCN-50%.
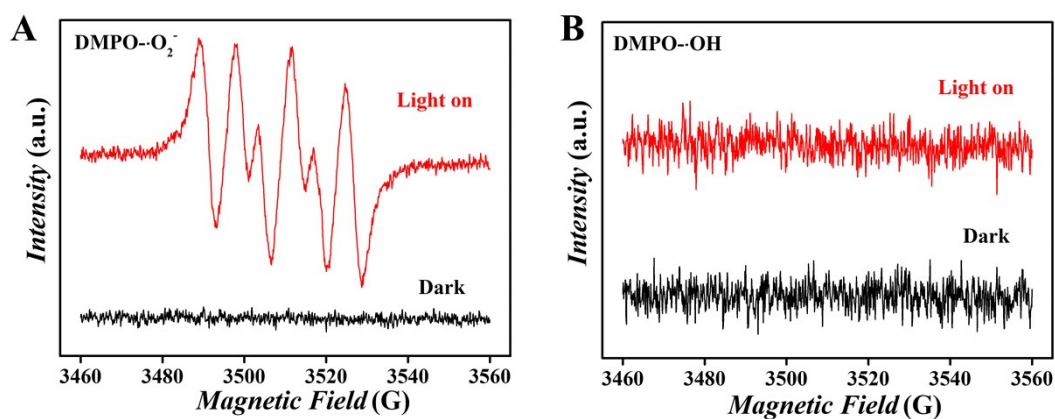
Fig. S9 DMPO spin-trapping ESR spectra for c-CSCN-50% in methanol dispersion (for DMPO-·O$_2^-$) and in aqueous dispersion (for DMPO-·OH) under visible-light irradiation.

Table S3 Comparison with other previous photocatalysts in the literature

Photocatalysts	concentration (mg L^{-1})	Dosage (g L^{-1})	Time (min)	Removal rate (%)	Light source	Reference
BFTO/Ag/UCN	20	0.5	100	86.0	300 W XL (λ > 400 nm)	[1]
CN/AC/GO	20	0.6	60	81.6	300 W XL (λ > 420 nm)	[2]
Ag/Ag$_2$O/PbBiO$_2$Br	20	1.0	120	84.4	300 W XL (λ > 420 nm)	[3]
Ag-AgVO$_3$/g-C$_3$N$_4$	300	0.2	120	83.6	300 W XL (λ > 410 nm)	[4]
BOB-R	30	0.2	60	86.4	86 W LED (λ = 420 nm)	[5]
h-BN/g-C$_3$N$_4$	10	1	60	79.7	300 W XL (λ > 420 nm)	[6]
3%NGQDs-60%C$_3$N$_4$ /Bi$_2$WO$_6$	10	0.5	90	85.2	250 W XL (λ > 420 nm)	[7]
Co$_3$O$_4$@CoO/g-C$_3$N$_4$	10	0.6	120	97.0	500 W XL	[8]
Co$_3$O$_4$/g-C$_3$N$_4$	15	0.4	60	92.6	500 W XL (λ = 420 nm)	[9]
c-CSCN	25	0.2	60	88.0	300 W XL (λ > 400 nm)	This work

BFTO: Bi$_5$FeTi$_3$O$_{15}$; g-C$_3$N$_4$: graphitic carbon nitride; UCN: ultrathin g-C$_3$N$_4$; CN: g-C$_3$N$_4$; AC: Ag$_2$CO$_3$; GO: graphene oxide; BOB-R: Bi$_{24}$O$_{31}$Br$_{10}$ (synthesized at room temperature); NGQDs: nitrogen-doped graphene quantum dots; c-CSCN: cage-Co$_9$S$_8$/g-C$_3$N$_4$; XL: Xenon lamp.
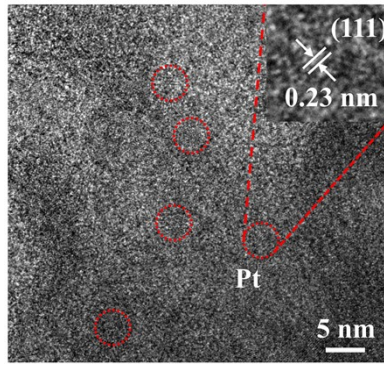
Fig. S10 HRTEM image showing Pt photodeposition on c-CSCN-50%.
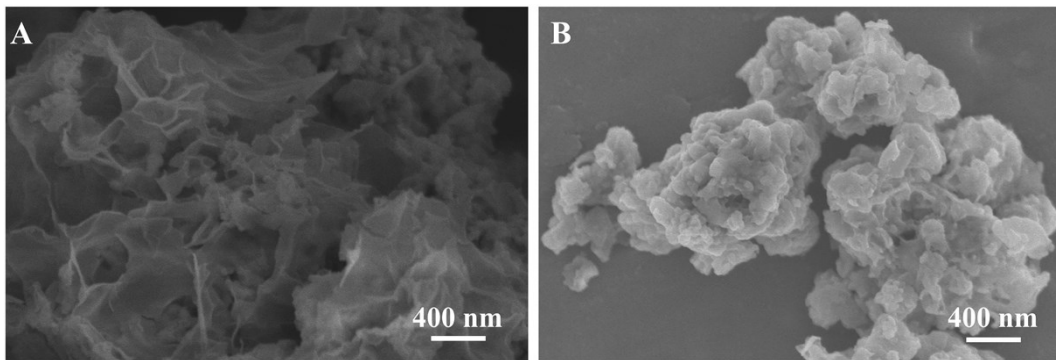
Fig. S11 SEM images of s-Co$_9$S$_8$ (A) and s-CSCN-50% (B).
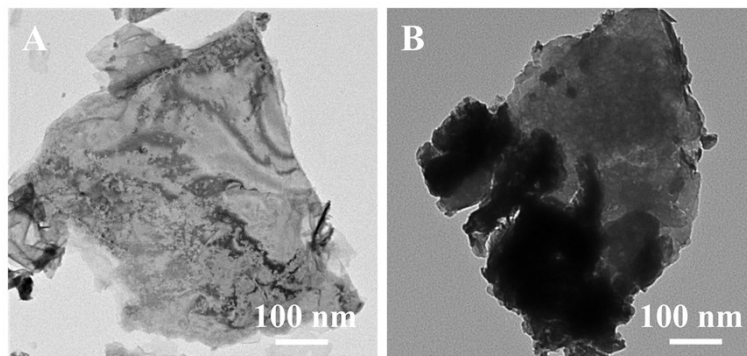
Fig. S12 TEM images of s-Co$_9$S$_8$ (A) and s-CSCN-50% (B).
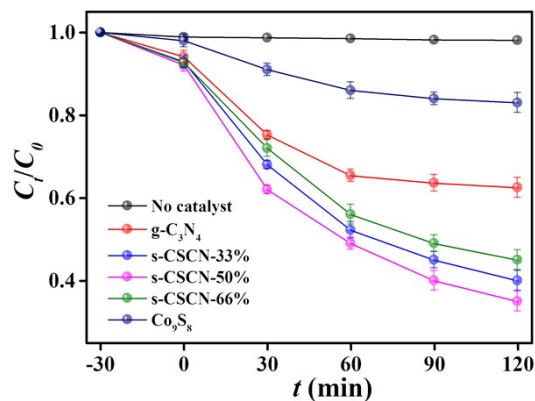
Fig. S13 Photodegradation of TC in different reaction systems.
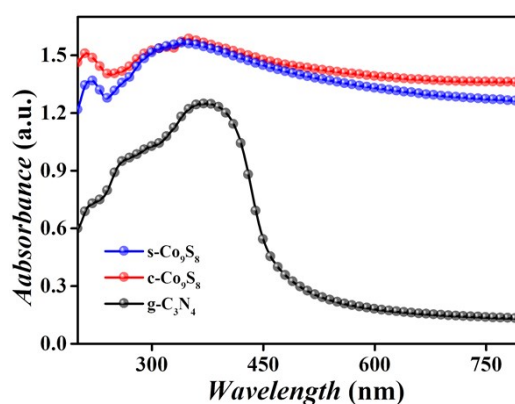
Fig. S14 UV-Vis diffuse reflectance spectra of g-C_3N_4, c-Co_9S_8 and s-Co_9S_8

References

[1] K. Wang, J. Li, G. Zhang, Ag-Bridged Z-Scheme 2D/2D $Bi_5FeTi_3O_{15}$/g-C_3N_4 Heterojunction for Enhanced Photocatalysis: Mediator-Induced Interfacial Charge Transfer and Mechanism Insights, ACS APPL MATER INTER, 11(2019) 27686-27696.

[2] H. Liu, C. Liang, C. Niu, D. Huang, Y. Du, H. Guo, L. Zhang, Y. Yang, G. Zeng, Facile assembly of g-C_3N_4/Ag_2CO_3/graphene oxide with a novel dual Z-scheme system for enhanced photocatalytic pollutant degradation, APPL. SURF. SCI., 475(2019) 421-434.

[3] H. Guo, C. Niu, D. Huang, N. Tang, C. Liang, L. Zhang, X. Wen, Y. Yang, W. Wang, G. Zeng, Integrating the plasmonic effect and p-n heterojunction into a novel Ag/Ag_2O/$PbBiO_2Br$ photocatalyst: Broadened light absorption and accelerated charge separation co-mediated highly efficient visible/NIR light photocatalysis, CHEM. ENG. J., 360(2019) 349-363.

[4] D. Chen, B. Li, Q. Pu, X. Chen, G. Wen, Z. Li, Preparation of Ag-$AgVO_3$/g-C_3N_4 composite photo-catalyst and degradation characteristics of antibiotics, J. HAZARD. MATER., 373(2019) 303-312.

[5] B. Xiao, W. Zhao, Y. Xiang, X. Wu, G. Zhang, Vis-NIR responsive $Bi_{24}O_{31}Br_{10}$ and corresponding composite with up-conversion phosphor towards efficient photocatalytic oxidation, APPL. SURF. SCI., 489(2019) 210-219.

[6] L. Jiang, X. Yuan, G. Zeng, Z. Wu, J. Liang, X. Chen, L. Leng, H. Wang, H. Wang, Metal-free

efficient photocatalyst for stable visible-light photocatalytic degradation of refractory pollutant, Applied Catalysis B: Environmental, 221(2018) 715-725.

[7] H. Che, C. Liu, W. Hu, H. Hu, J. Li, J. Dou, W. Shi, C. Li, H. Dong, NGQD active sites as effective collectors of charge carriers for improving the photocatalytic performance of Z-scheme g-C_3N_4/Bi_2WO_6 heterojunctions, CATAL SCI TECHNOL, 8(2018) 622-631.

[8] J. Zheng, L. Zhang, Designing 3D magnetic peony flower-like cobalt oxides/g-C_3N_4 dual Zscheme photocatalyst for remarkably enhanced sunlight driven photocatalytic redox activity, Chemical Engineering Journal, 369(2019) 947-956.

[9] W. Zhao, J. Li, T. She, S. Ma, Z. Cheng, G. Wang, P. Zhao, W. Wei, D. Xia, D. Leung, Study on the Photocatalysis Mechanism of the Z-Scheme Cobalt Oxide Nanocubes/Carbon Nitride Nanosheets Heterojunction Photocatalyst with High Photocatalytic Performances, Journal of Hazardous Materials, 402(2021) 123839.